

Large bulk photovoltaic effect and Fermi surface mediated its enhancement with chemical potential in ZnGeP₂

Banasree Sadhukhan^{1,2}

¹*Department of Physics and Nanotechnology, SRM Institute of Science and Technology, Kattankulathur, 603203, Chennai, Tamil Nadu, India**

²*Tata Institute of Fundamental Research, Hyderabad, Telangana 500046, India*

Bulk photovoltaic effect is a non-linear response in noncentrosymmetric materials that converts light into DC current. In this work, we investigate the optical linear and non-linear responses in a chalcopyrite semiconductor ZnGeP₂. We report large bulk photovoltaics namely shift and circular photogalvanic current conductivities which are $4.46 \mu\text{A}/\text{V}^2$ and $-5.49 \mu\text{A}/\text{V}^2$ respectively with the incident photo energy around ~ 5 eV at the chemical potential of $E_f = 0$ eV which increase about 38% and 81% respectively at a chemical potential of $E_f = 1.52$ eV. The systematic evolution of the bulk Fermi surface along with the high symmetry points in three dimensional Brillouin zone reveals the enhancement of bulk photovoltaics with the chemical potential in ZnGeP₂. To verify our findings, we further explore the distribution of bulk projected bands and surface Fermi surface distribution in the energy landscape using tight binding Hamiltonian within semi infinite slab geometry. This shows that the augmentation of bulk photovoltaics with the chemical potential is due to the surface Fermi surface states along the high symmetry $\Gamma - Z$ direction in Brillouin zone. Our thorough and detailed study not only provides a deeper understanding about the role of Fermi surface contribution to the bulk photovoltaic responses with chemical potential, but also suggests ZnGeP₂ as an ideal candidate for optoelectronics and bulk photovoltaics.

I. INTRODUCTION

Sustainable energy demands the development of new platforms for efficient solar energy conversion. The Shockley-Queisser limit constrains the performance of conventional solar cells based on p-n junctions, so alternative approaches are worth exploring. One of the most promising alternative sources of photocurrent is the bulk photovoltaic effect (BPVE) that produces photocurrents in materials lacking inversion symmetry and unlike conventional p-n junctions, the generated photovoltage is above the bandgap limit [1–13]. BPVE is a second-order nonlinear response, which can be decomposed into a linear photogalvanic effect (LPGE) and a circular photogalvanic effect (CPGE), respectively, based on the linear and circular polarization state of the incident light respectively [1, 2, 6–15]. The CPGE can be directly related to the Berry curvature of the Bloch bands involved in the optical transition and proportional to the topological charge of the Weyl semimetals [13]. Microscopically, the shift current (LPGE) originates from the shift of the wave packet of Bloch electrons during interband photoexcitation [12]. Therefore, The shift and circular photogalvanic (CPG) current originate from the interband Berry connections and Berry curvature of the Bloch bands during optical transition respectively [7, 11, 15].

Nonlinear responses open new opportunities for revealing the topology and band structure geometry in condensed matter systems [10, 16, 17]. For example, shift and circular photocurrents, nonlinear susceptibilities are being used as probes for the exploration of the crystallographic orientation, band structure geometry, grain

boundaries [11, 12, 14, 18–21], Hall effects in both time-reversal invariant and broken systems [8, 22–25]. The effects of the Fermi surface and disorder scattering on nonlinear optical response have started to gain attention very recently [23, 26–33]. Intrinsic contribution of Fermi surface, stemming from the photoinduced electronic transitions on the Fermi surface, to the BPVE has been reported in metallic systems under illumination by polarized light [27, 28]. The intrinsic/extrinsic contribution of Fermi surface means whether it is independent/dependent on scattering time. Interplay between band geometric quantities give rises to the second harmonic generation which produces resonant peaks in optical response for topological materials due to the effect of Fermi surface [29–32]. Recent studies have shown that subbandgap photocurrents due to band broadening in semiconductors and insulators can be used to measure finite lifetimes, in contrast to clean limit i.e., at zero temperature [33].

The fundamental requirement for a material to produce a current via the BPVE is the broken inversion symmetry which allows the asymmetric photoexcitation of charge carriers induced by electron-phonon or electron-electron scattering. BPVE has recently drawn attention in class of materials like hybrid perovskites, topological insulators, Weyl semimetals [7, 11, 34–36]. Chalcopyrite semiconductors have drawn attention for its potential application as a nonlinear optical material [9]. Therefore, they provide a new test bed to study BPVE as it includes both topological and non-topological materials [37, 38]. ZnGeP₂ is a one of the chalcopyrite semiconductor derived from zinc-blende III-V parent compound GaP where group III-Ga is replaced by group II-Zn and group IV-Ge atoms. In chalcopyrite structures, c/a ratio (where a , c are the lattice parameters) is slightly

* banasres@srmist.edu.in

lower than 2 compared to its ideal zinc-blende structures. This produces a compressive uniaxial strain which affects the Brillouin zone (BZ) of zinc-blende structures. The conduction-band minimum of the mother structure of GaP at X point in the BZ is folded onto the Γ point of the ZnGeP_2 [39]. Therefore, Γ point in the BZ has a strong impact on optical response of chalcopyrite compounds [39–44]. A model was proposed based on the splittings of the low-lying conduction-band states at Γ point in order to explain the strong peak in the photoluminescence spectra [40–42]. Controlled doping of Sc atoms in ZnGeP_2 move the chemical potential of 0.8 eV [45] above Fermi level.

In this work, we study the optical linear and non-linear response for a chalcopyrite semiconductor ZnGeP_2 . We use a recently developed multi-band approach collaborated with tight binding Wannier Hamiltonian to calculate BPVE. Using first-principles-based extensive calculations, we report a large bulk photovoltaics like shift and CPG current conductivities and its enhancement with chemical potential due to contribution of Fermi surface states around $\Gamma - Z$ direction in the BZ. The enhancements are 38% and 81% respectively for shift and CPG current conductivities at chemical potential of 1.52 eV around the peak of responses. The distribution of Fermi surface states in the projected energy landscape is also explored using tight binding Wannier Hamiltonian with semi-infinite slab geometry to examine microscopically the contribution Fermi surface states in the BZ on the enhancement of BPVE. The paper is organised as follows. In Sec. II we describe the computational details. In Sec. III we discuss our results on both linear optical response and bulk photovoltaic along with the electronic structure and enhancement of BPVE with chemical potential in ZnGeP_2 . Finally in Sec. IV, we conclude with future perspectives.

II. COMPUTATIONAL DETAILS

Chalcopyrite semiconductors crystallize into the tetragonal structure with a space group $I\bar{4}2d$. The atomic positions of ZnGeP_2 are Zn (0, 0, 0), Ge (0, 0, 0.5) and P (u, 0.25, 0.125), where u is the internal displacement parameter for the anion i.e., P atoms). The anion acquires an equilibrium position closer to one pair of cations as a result of dissimilar atoms as neighbors. The structural relaxation are done in Vienna Ab initio Simulation Package (VASP) with kpoints $12 \times 12 \times 12$ [46, 47]. The optimized lattice constants (a and c) and the internal structural parameter (u) are $a = 5.454 \text{ \AA}$, $c = 10.707 \text{ \AA}$ and $u = 0.267 \text{ \AA}$ respectively. The density functional theoretical calculations are performed with the optimized lattice parameters using the local density approximation (LDA) method as implemented within full-potential local-orbital (FPLO) code [48].

In the next step, we use a tight-binding model in the Wannier function basis to calculate the shift and CPG

current conductivities. The tight-binding model is obtained using maximally projected Wannier functions for the Zn-3d, 4s, Ge-3d, 4s, 4p and P-3s, 3p orbitals in the energy range of -9.0 to 5.0 eV. BZ was sampled by a $150 \times 150 \times 150$ k-mesh grid in BZ with satisfactory convergence to calculate shift and CPG current conductivities. This Wannier model is used further to calculate the spectral density for an infinite bulk system by k_z -integrating bulk projected band structure. Furthermore, a semi-infinite slab is set up to calculate spectral densities of [001]-surface. The spectral densities for both bulk and semi-infinite slab geometry are obtained using Green's function recursion method [49].

III. RESULTS AND DISCUSSION

A. Electronic structure

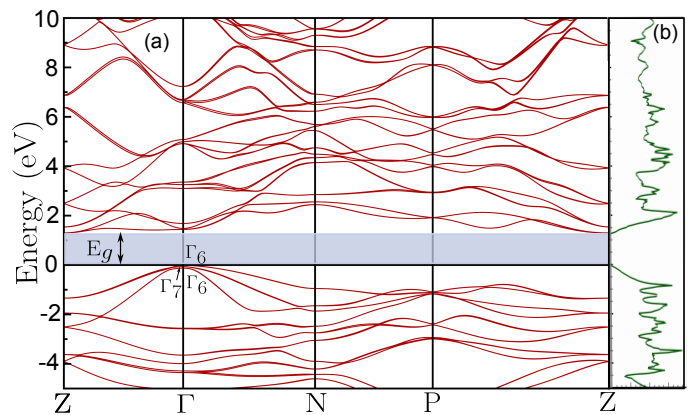


FIG. 1. (a) Band structure and (b) total density of states for ZnGeP_2 .

Figure 1 (a) represent the band structure along the high symmetry directions for ZnGeP_2 respectively. There is a remaining open question about the nature of its band gap whether it is direct, indirect or pseudo-direct because different studies lead to different results [39, 50–53]. The top of the valence band locates at Γ point and the bottom of the conduction band minimum locates at Z point. Therefore ZnGeP_2 has a indirect band gap of 1.32 eV from LSDA calculations. In comparing the with the experimental data, the calculated band gap is underestimated. It is obvious that the band gap calculated by density functional theory (DFT) is smaller than the one measured experimentally [54, 55]. This error is due to the discontinuity in different exchange-correlation potentials.

Without spin-orbit coupling, triply degenerated Γ_{15} valence band of its III–V zinc-blende compounds splits into a non-degenerate bands of Γ_4 and Γ_5 resulting a finite crystal field splitting ($\Delta_{cf} = E(\Gamma_5) - E(\Gamma_4)$) in chalcopyrite structures. In presence of spin-orbit interactions, Γ_5 splits into Γ_6 , Γ_7 and $\Gamma_4 \rightarrow \Gamma_6$ resulting Δ_{cf}

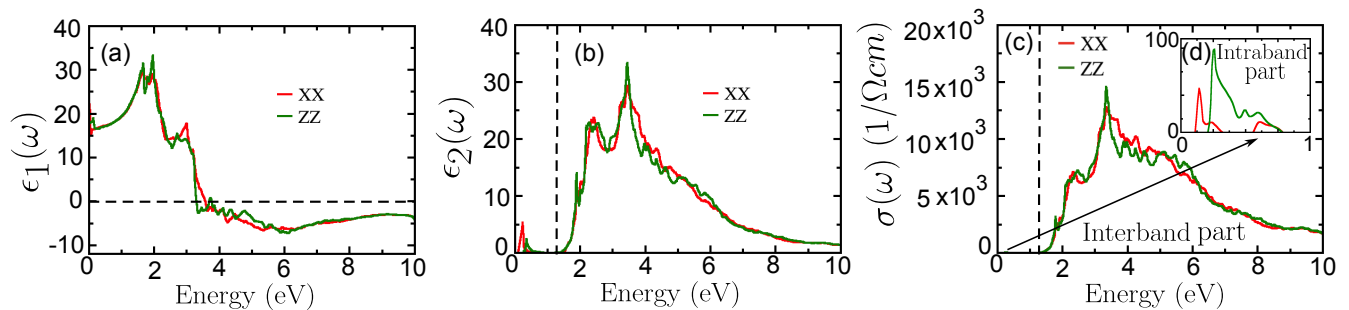


FIG. 2. (a) The real and (b) imaginary parts of the dielectric constant, and (c)-(d) optical conductivities as a function of the incident photon energy which show the intraband and interband parts for low and high incident photon energies respectively.

= $E(\Gamma_7) - E(\Gamma_6)$ [39, 56]. When the anion position parameter u of chalcopyrite crystal deviates from its ideal value i.e., 0.25, the absolute value of crystal field splitting increases. This is due to the deformation of the chalcopyrite materials compared to its parent zinc-blende structures. Therefore Δ_{cf} is zero in GaP, whereas it is of -102.5 meV for ZnGeP₂.

To get more insight into the the electronic structure, we look into the total (see Fig. 1(b)) and partial (see Fig. 4 in appendix) density of states of ZnGeP₂. The low-energy valence bands are mainly due to P-3p state with an admixture of Ge-4p and Zn-4p states, whereas Ge-4s, P-3d and Zn-4d states are also contributing to conduction band in addition to them. By analyzing the partial density states, one can clearly observe the strong effects of p-d hybridization which modifies the energy gap. The p-like states are pushed up and Zn-d like states are pushed down generating a band gap 1.32 eV for ZnGeP₂.

B. Linear optical response

The linear optical properties of ZnGeP₂ can be calculated from the complex dielectric function. In the presence of an electric field, the complex dielectric function can be divided into two parts: the intraband transition and the interband transition. In the case of metals, intraband transitions are useful, while in the case of semiconductors, interband transitions are useful. Interband transitions can be of two type, direct and indirect band transitions. Since the indirect interband transition contributes little to dielectric function which involves electron phonon scattering, therefore it can be ignored. By calculating the momentum matrix elements between occupied and unoccupied wave functions, the direct interband contribution can be calculated.

The optical properties within the linear response theory are obtained from the imaginary part of the dielectric

function is given by

$$\epsilon_2^{ij}(\omega) = \text{Im}[\epsilon_{ij}(\omega)] = -\frac{4\pi^2 e^2}{m_0^2 \omega^2} \int dk \sum_{n,l} (f_n - f_l) \times \frac{\langle \vec{k}_n | \hat{v}_i | \vec{k}_l \rangle \langle \vec{k}_l | \hat{v}_j | \vec{k}_n \rangle}{(E_{\vec{k}_n} - E_{\vec{k}_l} - \hbar\omega - i\delta)}, \quad (1)$$

where, $i, j = (x, y, z)$ are the Cartesian coordinates, $\hat{v}_i = \hat{p}_i/m_0$, m_0 is the free electron mass, $|\vec{k}_n\rangle$ are the wavefunction corresponding to the band with energy $E_{\vec{k}_n}$ at momentum \vec{k} and index n , $f_n \equiv f(E_{\vec{k}_n})$ is the Fermi function for the state with energy $E_{\vec{k}_n}$, and $\hbar\omega$ is the incident photon energy. $\delta = \hbar/\tau_s$ is the broadening parameter and depends inversely on the single particle relaxation time associated with the quantum mechanical broadening τ_s . The real part of the dielectric function can be obtained via the Kramers-Kronig relation:

$$\epsilon_1^{ij}(\omega) = \text{Re}[\epsilon_{ij}(\omega)] = \delta_{ij} + \frac{1}{\pi} \mathcal{P} \int_{-\infty}^{\infty} d\omega' \frac{\text{Im}[\epsilon_{ij}(\omega')]}{\omega - \omega'}. \quad (2)$$

The optical conductivity ($J_i = \sigma_{ij} \mathcal{E}_j$) is given by :

$$\sigma_{ij}(\omega) = \frac{\omega \epsilon_2^{ij}(\omega)}{4\pi}. \quad (3)$$

where J_k is the photocurrent generated by an electrical field \mathcal{E}_j .

Figure 2 represents the linear optical responses in ZnGeP₂. Tetragonal symmetry in ZnGeP₂ allows two independent linear optical components i.e one in-plane ($ij = xx = yy$) and one out-of-plane ($ij = zz$) components. Figure 2(a)-(b) represent the real and imaginary parts of the dielectric function for ZnGeP₂. $\epsilon_1(\omega)$ has a peak with a magnitude of 33.02 at 1.98 eV. Then it sharply decreases between 1.98 eV and 3.36 eV and, becomes negative after that. The minimum of $\epsilon_1(\omega)$ occurs at 6.02 eV followed by a slow increasing trends toward zero. The static dielectric constant is $\epsilon_1(0) = 18.01$ for ZnGeP₂. $\epsilon_2(\omega)$ shows that the threshold energy of the dielectric function occurs at 1.32 eV i.e above the band gap. The imaginary part of the dielectric constant $\epsilon_2(\omega)$ shows peaks at 2.41 and 3.44 eV respectively. The small

contributions of $\epsilon_2(\omega)$ below band gap originates from the intraband transitions of optical response [57, 58].

The calculated linear optical conductivities are presented in Fig.2(c)-(d). The total conductivity has contributions from both interband and intraband processes i.e, $\sigma(\omega) = \sigma_{\text{interband}}(\omega) + \sigma_{\text{intra}}(\omega)$. The optical transitions from valence to conduction bands lead to interband optical conductivity above the band gap in ZnGeP₂. Therefore, $\sigma(\omega)$ produces a strong peak at 3.34 eV followed by a weak peak at 2.32 eV due to interband optical transition as shown in Fig.2(c). The intraband optical conductivity below band gap for ZnGeP₂ originates from Drude like conductivity due to free carriers as shown in Fig.2(d).

C. Bulk photovoltaics and effect of Fermi surface with chemical potential

For the bulk photovoltaic responses, the photoconductivity in quadratic response theory appears as [7, 9, 59, 60]:

$$\sigma_{ij}^k = \frac{|e|^3}{8\pi^3\omega^2} \text{Re} \left\{ \phi_{ij} \sum_{\Omega=\pm\omega} \sum_{l,m,n} \int_{BZ} dk (f_l - f_n) \right. \\ \left. \times \frac{\langle \vec{k}_n | \hat{v}_i | \vec{k}_l \rangle \langle \vec{k}_l | \hat{v}_j | \vec{k}_m \rangle \langle \vec{k}_m | \hat{v}_k | \vec{k}_n \rangle}{(E_{\vec{k}_n} - E_{\vec{k}_m} - i\delta)(E_{\vec{k}_n} - E_{\vec{k}_l} + \hbar\Omega - i\delta)} \right\}. \quad (4)$$

The conductivity σ_{ij}^k ($i, j, k = x, y, z$) is a third rank tensor representing the photocurrent J_k generated by an electrical field via $J_k = \sigma_{ij}^k \mathcal{E}_i^* \mathcal{E}_j$. ϕ_{ij} is the phase difference between the driving fields \mathcal{E}_i and \mathcal{E}_j . The real (imaginary) part of the integral in Eq. (4) describes the shift (CPG) current conductivity under linearly (circularly) polarized light respectively.

Now we study the non-linear photocurrent responses under linearly and circularly polarized light respectively for different chemical potentials. As the photocurrent response arises from both real and virtual band transitions, it is generally strongly dependent on the incident photon energy. As we consider the relaxation time approximation, therefore we used broadening parameter $\delta = 10$ meV in our calculations. Chalcopyrite semiconductors belong to $D_{2d}(-4m2)$ point group. Therefore, the second order photoconductivity (σ_{ij}^k) tensor has the form :

$$\sigma_{ij}^k = \begin{pmatrix} 0 & 0 & 0 & \sigma_{yz}^x & 0 & 0 \\ 0 & 0 & 0 & 0 & \sigma_{xz}^y & 0 \\ 0 & 0 & 0 & 0 & 0 & \sigma_{xy}^z \end{pmatrix}$$

ZnGeP₂ has the mirror reflection M_{xy} in the xy plane and $M_{xy} = M_{yx}$. It also has the 4_2 screw rotational symmetry about the z axis which gives $\sigma_{yz}^x = \sigma_{xz}^y$. Therefore, the two independent components in nonlinear optical photoconductivity tensor are σ_{yz}^x and σ_{xy}^z . For σ_{yz}^x , the current responses are along the x direction for yz polarization of light.

Figure 3(a) presents the calculated shift current conductivity (σ_{yz}^x component of second order photoconductivity tensor) under linear polarization of light for different chemical potentials E_f . The shift current conductivity get a value of $-3.75 \mu\text{A}/\text{V}^2$ at the incident photo energy of ~ 4 eV when the chemical potential is at 0 eV. By shifting it to $E_f = 1.52$ eV, σ_{yz}^x reaches to a value to $-5.19 \mu\text{A}/\text{V}^2$. Further shifting of chemical potential at $E_f = 1.68$ eV, shift current conductivity is slightly drop down to $-4.59 \mu\text{A}/\text{V}^2$. The shift current conductivity gets inverted above the incident energy of 4.8 eV and reaches to a peak value of $4.46 \mu\text{A}/\text{V}^2$ at $E_f = 0$ eV which is an order of magnitude larger than BPVE in multiferroic material BiFeO₃ [18]. However, the σ_{yz}^x enhances to 6.17 and $5.82 \mu\text{A}/\text{V}^2$ for $E_f = 1.52$ eV and 1.68 eV respectively. The shift current conductivity has positive magnitude for the incident energy windows of (4.8-9.7) eV and gets inverted otherwise. The nature of the response is same for all chemical potentials but the contributions to responses can vary significantly across the BZ for a given chemical potential E_f as shown in Fig. 3(a).

Figure 3(b) shows the calculated CPG current conductivity (σ_{yz}^x component of second order photoconductivity tensor) for different chemical potentials E_f . The CPG current conductivity at incident photo energies near the band gap is small. It reaches a maximum value of $-1.51 \mu\text{A}/\text{V}^2$ at 2.32 eV within visible energy spectrum. CPG current conductivity is negative just above band gap and reverses its direction resulting in a peak of $2.35 \mu\text{A}/\text{V}^2$ at 3.8 eV followed by a broad peak of $-5.49 \mu\text{A}/\text{V}^2$ at 4.8 eV for chemical potential $E_f = 0$ eV. Shifting chemical potential has a large effects also on CPG current conductivity. However, the CPG current conductivity reaches to -9.95 and $-10.76 \mu\text{A}/\text{V}^2$ at incident photon energy of 4.8 eV for $E_f = 1.52$ eV and 1.68 eV respectively. σ_{xy}^z part for second order shift and CPG current conductivities are presented in appendix (see Fig.5). However, σ_{yz}^x component contributes more than σ_{xy}^z component to BPVE in ZnGeP₂ which means BPVE with yz polarization of light is higher in ZnGeP₂ than xy polarization of light.

Fermi surface has an intrinsic contribution to BPVE [27]. Both the shift and CPG current conductivities enhance by shifting the chemical potential above band gap to (1.52 - 1.68) eV as shown in Fig.3(a)-(b). Both the shift and CPG current conductivities get its maximum value of $6.17 \mu\text{A}/\text{V}^2$ and $-10.76 \mu\text{A}/\text{V}^2$ respectively for chemical potential $E_f = 1.52$ eV. To investigate the connection of photovoltaic effect to Fermi surface for ZnGeP₂, we study the three dimensional (3D) bulk Fermi surface at different chemical potentials in the whole BZ. Figure 5(a)-(h) (in appendix) present the systematic evolution of the bulk 3D Fermi surface along with the high symmetry points in BZ by changing the chemical potential E_f from 1.33 to 2.15 eV above the band gap.

When the chemical potential touches at the conduction band just above the band gap ($E_f = 1.33$ eV), the contribution of the Fermi surface appears at high sym-

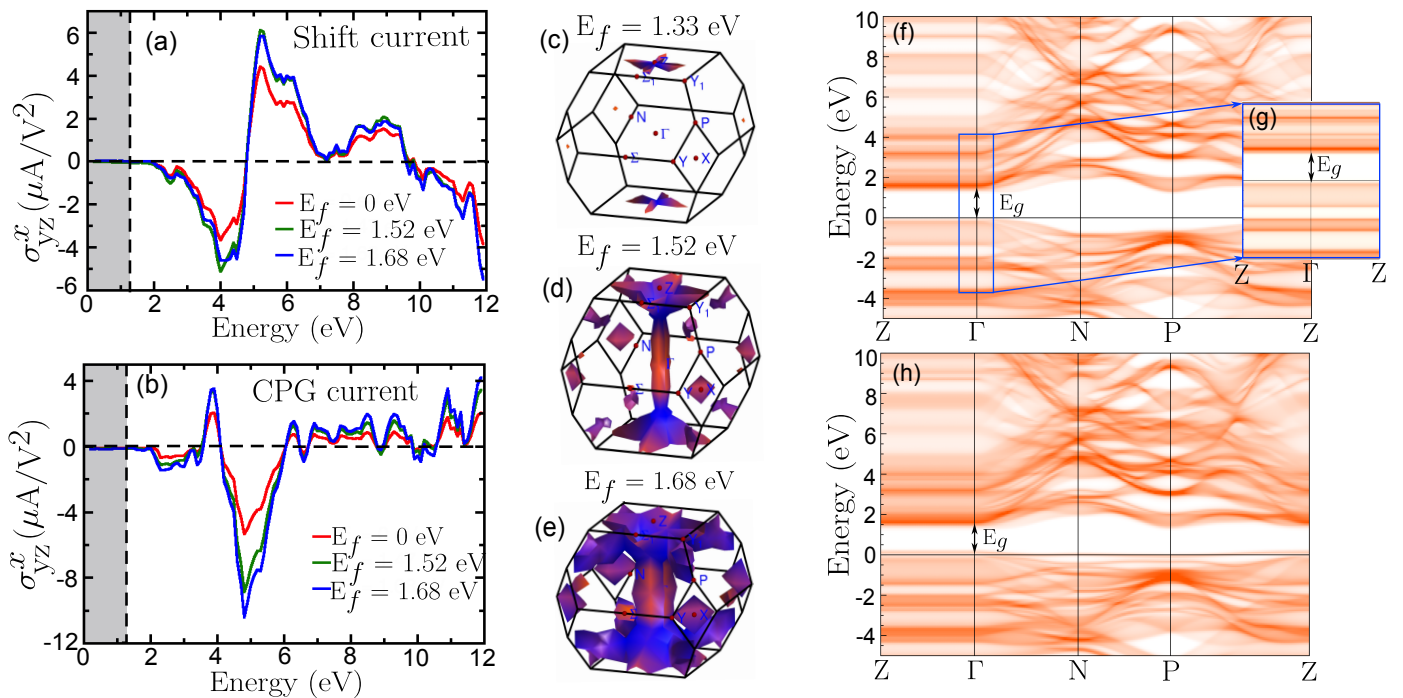


FIG. 3. Fermi surface mediated enhancement of bulk photovoltaic effects for (a) shift current conductivity and (b) CPG current conductivity with different chemical potentials E_f . (c)-(e) The bulk Fermi surface states in full Brillouin zone indicating high symmetry points for different chemical potentials E_f . (f)-(g) k_z -integrated [(001)-direction] bulk projected bands. (h) Energy distribution curve for [001]-surface in semi infinite slab.

metry Z point as shown Fig.3(c). Further shifting of the chemical potential to $E_f = 1.52$ eV, the bulk 3D Fermi surface appears along the high symmetry line $\Gamma - Z$ directions instead of a small contribution only at Z point as shown in Fig. 3(d). The appearance of the bulk 3D Fermi surface broadens at the chemical potential $E_f = 1.68$ eV (see Fig. 3(e)). This enhances the both the shift and CPG current conductivities when the chemical potential are between (1.52 - 1.68) eV for ZnGeP_2 due to contribution of Fermi surface states along $\Gamma - Z$ direction to non-linear photocurrent. If we further move the chemical potential above $E_f = 1.68$ eV, the contribution of the bulk 3D Fermi surface in the BZ decreases along $\Gamma - Z$ direction (see 5 (e)-(h) in appendix) which results again decrease of both shift and CPG current conductivities in ZnGeP_2 .

The non-linear photo current conductivities (shift and CPG current) are forbidden below the band i.e 1.32 eV. The peak of non-linear responses appear a few eV above the band gap and outside the visible energy window. The underestimation of band gap in semiconductors within DFT by the local and semi-local functionals is a common issue which could be solved under the treatment of DFT with Hubbard U approximation or using different hybrid functionals. ZnGeP_2 has a band gap 2.06 eV using HSE06 hybrid functional which is close to experimental value of 2.05 eV [54, 55, 61]. Now the question arises on how the calculated optical responses are justified within DFT calculations. This band gap deficiency is also ad-

ressed by shifting the conduction bands rigidly (called scissor shift) such that the electronic band gap matches with the experimental value using a “scissors operation” on the standard DFT bands [9, 62, 63]. Therefore under the “scissors operation”, there will be scissor shift of 0.74 eV to DFT band gap to match with experimental value for ZnGeP_2 .

By implementing the procedure of “scissors operation”, the optical response obtained from DFT is shifted by the same amount of scissor shift while maintaining the features of standard DFT [9, 64]. In a very recent work, we showed that the underlying features of band structures, hence optical and bulk photovoltaics responses remain same from two methods, DFT + scissor shift and DFT+ U , for another material ZnSnP_2 in the same chalcopyrite semiconductor series [9]. Only there is a rigid shift of the incident photon energy in optical and bulk photovoltaics responses above which the responses start [9]. It implies that under “scissors operation” the optical and bulk photovoltaics responses (DFT+scissor shift) retains the same features obtained from DFT with hybrid functional. The qualitative features of optical responses from both DFT+scissor shift and DFT with hybrid functional remain unchanged for ZnGeP_2 .

To investigate further, we also study surface Fermi surface states distribution in the projected energy landscape using tight binding Wannier Hamiltonian along with the momentum space 3D BZ. Figure 3(f)-(g) and (h) present the k_z -integrated projected band in bulk

and semi-infinite slab geometry respectively. The surface Fermi surface states available along $Z \leftarrow \Gamma \rightarrow Z$ direction at chemical potential around $E_f = 1.52$ eV above the band gap is due to the projection of bulk 3D Fermi surface (see Fig. 3 (d)-(e)) which contributes in the enhancement of BPVE in ZnGeP_2 . However, these states decrease after $E_f = 1.7$ eV.

IV. CONCLUSION

Chalcopyrite semiconductors provide a promising platform for observing bulk photovoltaics responses in addition to the linear response. We study the Fermi surface contribution to nonlinear DC photocurrent, namely shift and CPG current. We find that the polarized light induces electronic transitions on the Fermi surface that contribute to the enhancement of BPVE in ZnGeP_2 . The shift current and CPG current conductivities are 4.46 and $-5.49 \mu\text{A}/\text{V}^2$ with the incident photo energy at 4.8 eV for the chemical potential $E_f = 0$ eV which produces conductivities of 6.17 and $-9.95 \mu\text{A}/\text{V}^2$ respectively by shifting the chemical potentials E_f to 1.52 eV. We report the enhancement of shift and CPG current conductivities are about 38% and 81% due to Fermi surface states along the high symmetry $\Gamma - Z$ direction in momentum space BZ.

Our study is further collaborated by searching the sur-

face Fermi surface states in energy distribution landscape which produces intrinsic contribution to BPVE. In addition to non-linear responses, we also study the linear optical responses in ZnGeP_2 . Optical conductivity produces a peak of $14.83 \times 10^3 \Omega \cdot \text{cm}^{-1}$ at the incident photo energy of 3.35 eV. Relying on these in-depth understandings of the role of Fermi surface effects and the prediction of enhancement of BPVE due to surface Fermi surface states, ZnGeP_2 appears as a promising candidate for optoelectronic applications based on bulk photovoltaics. Our study also shed light on the root of enhanced efficiency for BPVE in noncentrosymmetric materials that could be controlled using chemical potentials. We believe that the results presented in our work will serve as a guide for both theory and experiment in the development and optimization of the next generation bulk photovoltaics using chalcopyrite materials [9].

V. ACKNOWLEDGEMENT

BS acknowledges Department of Science and Technology, Government of India, for financial support with reference no DST/WISE-PDF/PM-4/2023 under WISE Post-Doctoral Fellowship programme to carry out this work. We acknowledge IFW Dresden cluster and Ulrike Nitzsche for technical support.

-
- [1] Subhajit Pal, S Muthukrishnan, Banasree Sadhukhan, Sarath NV, D Murali, and Pattukkannu Murugavel, "Bulk photovoltaic effect in batio3-based ferroelectric oxides: An experimental and theoretical study," *Journal of Applied Physics* **129** (2021).
 - [2] F. Nastos and J. E. Sipe, "Optical rectification and shift currents in gaas and gap response: Below and above the band gap," *Phys. Rev. B* **74**, 035201 (2006).
 - [3] Andreas Pusch, Udo Römer, Dimitrie Culcer, and Nicholas J. Ekins-Daukes, "Energy conversion efficiency of the bulk photovoltaic effect," *PRX Energy* **2**, 013006 (2023).
 - [4] Congcong Le, Yang Zhang, Claudia Felser, and Yan Sun, "Ab initio study of quantized circular photogalvanic effect in chiral multifold semimetals," *Phys. Rev. B* **102**, 121111 (2020).
 - [5] Urmimala Dey, Jeroen van den Brink, and Rajyavardhan Ray, "Correlation between electronic polarization and shift current in cubic and hexagonal semiconductors LiZnx ($x = \text{P, As, Sb}$)," *Phys. Rev. Mater.* **8**, 025001 (2024).
 - [6] F. Nastos and J. E. Sipe, "Optical rectification and current injection in unbiased semiconductors," *Phys. Rev. B* **82**, 235204 (2010).
 - [7] Yang Zhang, Hiroaki Ishizuka, Jeroen van den Brink, Claudia Felser, Binghai Yan, and Naoto Nagaosa, "Photogalvanic effect in weyl semimetals from first principles," *Phys. Rev. B* **97**, 241118 (2018).
 - [8] Banasree Sadhukhan and Tanay Nag, "Role of time reversal symmetry and tilting in circular photogalvanic responses," *Phys. Rev. B* **103**, 144308 (2021).
 - [9] Banasree Sadhukhan, Yang Zhang, Rajyavardhan Ray, and Jeroen van den Brink, "First-principles calculation of shift current in chalcopyrite semiconductor znsp_2 ," *Phys. Rev. Mater.* **4**, 064602 (2020).
 - [10] Banasree Sadhukhan and Tanay Nag, "Electronic structure and unconventional nonlinear response in double weyl semimetal Srsi_2 ," *Phys. Rev. B* **104**, 245122 (2021).
 - [11] Steve M. Young and Andrew M. Rappe, "First principles calculation of the shift current photovoltaic effect in ferroelectrics," *Phys. Rev. Lett.* **109**, 116601 (2012).
 - [12] Takahiro Morimoto and Naoto Nagaosa, "Topological nature of nonlinear optical effects in solids," *Science Advances* **2**, e1501524 (2016).
 - [13] Fernando de Juan, Adolfo G. Grushin, Takahiro Morimoto, and Joel E. Moore, "Quantized circular photogalvanic effect in weyl semimetals," *Nature Communications* **8**, 15995 (2017).
 - [14] J. E. Sipe and A. I. Shkrebtii, "Second-order optical response in semiconductors," *Phys. Rev. B* **61**, 5337-5352 (2000).
 - [15] Takahiro Morimoto and Naoto Nagaosa, "Topological aspects of nonlinear excitonic processes in noncentrosymmetric crystals," *Phys. Rev. B* **94**, 035117 (2016).
 - [16] J. Orenstein, J. E. Moore, T. Morimoto, D. H. Torchinsky, J. W. Harter, and D. Hsieh, "Topology and symmetry of quantum materials via nonlinear optical re-

- sponses,” *Annual Review of Condensed Matter Physics* **12**, 247–272 (2021).
- [17] E. J. König, M. Dzero, A. Levchenko, and D. A. Pesin, “Gyrotropic hall effect in berry-curved materials,” *Phys. Rev. B* **99**, 155404 (2019).
- [18] Steve M. Young, Fan Zheng, and Andrew M. Rappe, “First-principles calculation of the bulk photovoltaic effect in bismuth ferrite,” *Phys. Rev. Lett.* **109**, 236601 (2012).
- [19] Ashley M. Cook, Benjamin M. Fregoso, Fernando de Juan, Sinisa Coh, and Joel E. Moore, “Design principles for shift current photovoltaics,” *Nature Communications* **8**, 14176 (2017).
- [20] Bruno R. Carvalho, Yuanxi Wang, Kazunori Fujisawa, Tianyi Zhang, Ethan Kahn, Ismail Bilgin, Pulickel M. Ajayan, Ana M. de Paula, Marcos A. Pimenta, Swastik Kar, Vincent H. Crespi, Mauricio Terrones, and Leandro M. Malard, “Nonlinear dark-field imaging of one-dimensional defects in monolayer dichalcogenides,” *Nano Letters* **20**, 284–291 (2020).
- [21] Xiaobo Yin, Ziliang Ye, Daniel A. Chenet, Yu Ye, Kevin O’Brien, James C. Hone, and Xiang Zhang, “Edge nonlinear optics on a mos2 atomic monolayer,” *Science* **344**, 488–490 (2014).
- [22] Pankaj Bhalla, Ming-Xun Deng, Rui-Qiang Wang, Lan Wang, and Dimitrie Culcer, “Nonlinear ballistic response of quantum spin hall edge states,” *Phys. Rev. Lett.* **127**, 206801 (2021).
- [23] Z. Z. Du, C. M. Wang, Shuai Li, Hai-Zhou Lu, and X. C. Xie, “Disorder-induced nonlinear hall effect with time-reversal symmetry,” *Nature Communications* **10**, 3047 (2019).
- [24] S. Nandy and Inti Sodemann, “Symmetry and quantum kinetics of the nonlinear hall effect,” *Phys. Rev. B* **100**, 195117 (2019).
- [25] Banasree Sadhukhan and Tanay Nag, “Effect of chirality imbalance on hall transport of prrh₂,” *Phys. Rev. B* **107**, L081110 (2023).
- [26] Jorge I. Facio, Dmitri Efremov, Klaus Koepnik, Jih-Shih You, Inti Sodemann, and Jeroen van den Brink, “Strongly enhanced berry dipole at topological phase transitions in bitei,” *Phys. Rev. Lett.* **121**, 246403 (2018).
- [27] Lingyuan Gao, Zachariah Addison, E. J. Mele, and Andrew M. Rappe, “Intrinsic fermi-surface contribution to the bulk photovoltaic effect,” *Phys. Rev. Res.* **3**, L042032 (2021).
- [28] Zaiyao Fei, Wenjin Zhao, Tauno A. Palomaki, Bosong Sun, Moira K. Miller, Zhiying Zhao, Jiaqiang Yan, Xiaodong Xu, and David H. Cobden, “Ferroelectric switching of a two-dimensional metal,” *Nature* **560**, 336–339 (2018).
- [29] G. Lefkidis and W. Hübner, “Phononic effects and non-locality contributions to second harmonic generation in nio,” *Phys. Rev. B* **74**, 155106 (2006).
- [30] Zhi Li, Ya-Qin Jin, Takami Tohyama, Toshiaki Iitaka, Jiu-Xing Zhang, and Haibin Su, “Second harmonic generation in the weyl semimetal taas from a quantum kinetic equation,” *Phys. Rev. B* **97**, 085201 (2018).
- [31] Pankaj Bhalla, Kamal Das, Dimitrie Culcer, and Amit Agarwal, “Resonant second-harmonic generation as a probe of quantum geometry,” *Phys. Rev. Lett.* **129**, 227401 (2022).
- [32] Pankaj Bhalla, Allan H. MacDonald, and Dimitrie Culcer, “Resonant photovoltaic effect in doped magnetic semiconductors,” *Phys. Rev. Lett.* **124**, 087402 (2020).
- [33] Daniel Kaplan, Tobias Holder, and Binghai Yan, “Non-vanishing subgap photocurrent as a probe of lifetime effects,” *Phys. Rev. Lett.* **125**, 227401 (2020).
- [34] Liang Z. Tan and Andrew M. Rappe, “Enhancement of the bulk photovoltaic effect in topological insulators,” *Phys. Rev. Lett.* **116**, 237402 (2016).
- [35] Kun Woo Kim, Takahiro Morimoto, and Naoto Nagaosa, “Shift charge and spin photocurrents in dirac surface states of topological insulator,” *Phys. Rev. B* **95**, 035134 (2017).
- [36] Xiao Jiang, Liangting Ye, Xiaoqiang Wu, Lei Kang, and Bing Huang, “Role of large rashba spin-orbit coupling in second-order nonlinear optical effects of polar bib₃o₆,” *Phys. Rev. B* **106**, 195126 (2022).
- [37] Wanxiang Feng, Di Xiao, Jun Ding, and Yugui Yao, “Three-dimensional topological insulators in I–III–v₂ and II–IV–v₂ chalcopyrite semiconductors,” *Phys. Rev. Lett.* **106**, 016402 (2011).
- [38] Surasree Sadhukhan, Banasree Sadhukhan, and Sudipta Kanungo, “Pressure-driven tunable properties of the small-gap chalcopyrite topological quantum material zn₂sb₂: A first-principles study,” *Phys. Rev. B* **106**, 125112 (2022).
- [39] Sukit Limpijumnong, Walter R. L. Lambrecht, and Benjamin Segall, “Electronic structure of zn₂ge₂: a detailed study of the band structure near the fundamental gap and its associated parameters,” *Phys. Rev. B* **60**, 8087–8096 (1999).
- [40] Yurri V. Rud, Vasilii Yu, M. C. Ohmer, and P. G. Shunemann, “Photoluminescence study of p-zn₂ge₂ crystals,” *MRS Online Proceedings Library* **450**, 339–344 (1996).
- [41] MC Petcu, NC Giles, PG Schunemann, and TM Polak, “Band-edge photoluminescence at room temperature from zn₂ge₂ and ag₂ge₂,” *physica status solidi (b)* **198**, 881–888 (1996).
- [42] JE McCrae Jr, MR Gregg, RL Hengehold, YK Yeo, PH Ostdiek, MC Ohmer, PG Schunemann, and TM Polak, “Polarized luminescence study of ordered nonlinear optical material zn₂ge₂,” *Applied physics letters* **64**, 3142–3144 (1994).
- [43] Guy Fishman and Bernard Sermage, “Structure of the *d* level and the *p* – *d* coupling in i-iii-v₂ chalcopyrite compounds,” *Phys. Rev. B* **18**, 7099–7103 (1978).
- [44] J. E. Jaffe and Alex Zunger, “Electronic structure of the ternary pnictide semiconductors zn₂sp₂, zn₂ge₂, zn₂sn₂, zn₂si₂, and mgsip₂,” *Phys. Rev. B* **30**, 741–756 (1984).
- [45] Vladimir I Voevodin, Valentin N Brudnyi, Yury S Sarkisov, Xinyang Su, and Sergey Yu Sarkisov, “Electrical relaxation and transport properties of zn₂ge₂ and 4h-sic crystals measured with terahertz spectroscopy,” in *Photonics*, Vol. 10 (MDPI, 2023) p. 827.
- [46] G. Kresse and J. Furthmüller, “Efficient iterative schemes for ab initio total-energy calculations using a plane-wave basis set,” *Phys. Rev. B* **54**, 11169–11186 (1996).
- [47] G. Kresse and J. Hafner, “Ab initio molecular dynamics for liquid metals,” *Phys. Rev. B* **47**, 558–561 (1993).
- [48] Klaus Koepnik and Helmut Eschrig, “Full-potential nonorthogonal local-orbital minimum-basis band-structure scheme,” *Phys. Rev. B* **59**, 1743–1757 (1999).
- [49] MP Lopez Sancho, JM Lopez Sancho, JM Lopez Sancho, and J Rubio, “Highly convergent schemes for the calculation of bulk and surface green functions,” *Journal of Physics F: Metal Physics* **15**, 851 (1985).

- [50] R Bendorius, VD Prochukhan, and A Šileika, “The lowest conduction band minima of a2b4c-type semiconductors,” *physica status solidi (b)* **53**, 745–752 (1972).
- [51] J. L. Shay, B. Tell, E. Buehler, and J. H. Wernick, “Band structure of zngep₂ and znsip₂ — ternary compounds with pseudodirect energy gaps,” *Phys. Rev. Lett.* **30**, 983–986 (1973).
- [52] F. Chiker, B. Abbar, S. Bresson, B. Khelifa, C. Mathieu, and A. Tadjer, “The reflectivity spectra of znxp₂ (x=si, ge, and sn) compounds,” *Journal of Solid State Chemistry* **177**, 3859–3867 (2004).
- [53] SR Zhang, LH Xie, SD Ouyang, XW Chen, and KH Song, “Electronic structure, chemical bonding and optical properties of the nonlinear optical crystal zngep₂ by first-principles calculations,” *Physica Scripta* **91**, 015801 (2015).
- [54] Joseph Leo Shay and Jack Harry Wernick, *Ternary chalcopyrite semiconductors: growth, electronic properties, and applications: international series of monographs in the science of the solid state*, Vol. 7 (Elsevier, 2013).
- [55] A MacKinnon, in: *Numerical Data and Functional Relationships in Science and Technology, Landolt-Bornstein New Series, Group III, vol. 17, Pt. H, p. 9 (ed.) O Madelung* (Berlin: Springer, 1985).
- [56] V. N. Brudny[˘]i, V. G. Voevodin, and S. N. Grinyaev, “Deep levels of intrinsic point defects and the nature of “anomalous” optical absorption in zngep₂,” *Physics of the Solid State* **48**, 2069–2083 (2006).
- [57] Shalika R Bhandari, DK Yadav, BP Belbase, M Zeeshan, B Sadhukhan, DP Rai, RK Thapa, GC Kaphle, and Madhav Prasad Ghimire, “Electronic, magnetic, optical and thermoelectric properties of ca 2 cr 1- x ni x oso 6 double perovskites,” *RSC advances* **10**, 16179–16186 (2020).
- [58] Souvik Biswas, William S Whitney, Meir Y Grajower, Kenji Watanabe, Takashi Taniguchi, Hans A Bechtel, George R Rossman, and Harry A Atwater, “Tunable intraband optical conductivity and polarization-dependent epsilon-near-zero behavior in black phosphorus,” *Science advances* **7**, eabd4623 (2021).
- [59] Wolfgang Kraut and Ralph von Baltz, “Anomalous bulk photovoltaic effect in ferroelectrics: A quadratic response theory,” *Phys. Rev. B* **19**, 1548–1554 (1979).
- [60] Ralph von Baltz and Wolfgang Kraut, “Theory of the bulk photovoltaic effect in pure crystals,” *Phys. Rev. B* **23**, 5590–5596 (1981).
- [61] ShunRu Zhang, DuoPeng Zeng, HaiJun Hou, and You Yu, “First-principles prediction on elastic anisotropic, optical, lattice dynamical properties of zngep 2,” *Indian Journal of Physics* **94**, 1335–1341 (2020).
- [62] R. W. Godby, M. Schlüter, and L. J. Sham, “Self-energy operators and exchange-correlation potentials in semiconductors,” *Phys. Rev. B* **37**, 10159–10175 (1988).
- [63] Zachary H. Levine and Douglas C. Allan, “Linear optical response in silicon and germanium including self-energy effects,” *Phys. Rev. Lett.* **63**, 1719–1722 (1989).
- [64] F. Nastos, B. Olejnik, K. Schwarz, and J. E. Sipe, “Scissors implementation within length-gauge formulations of the frequency-dependent nonlinear optical response of semiconductors,” *Phys. Rev. B* **72**, 045223 (2005).

VI. APPENDIX

Figure 4 represents the orbital projected partial density of states for different atoms for ZnGeP₂. Figure 5 represents σ_{xy}^z component of shift and CPG current conductivities for different chemical potentials E_f . The peak of response for the shift current and CPG current conductivities are -1.69 and -0.92 $\mu\text{A}/\text{V}^2$ at the chemical potential of $E_f = 0$ which are -2.88 and -2.38 $\mu\text{A}/\text{V}^2$ at the chemical potential of $E_f = 1.52$ eV. Figure 6(a)-(h) show the calculated bulk 3D Fermi surface distribution in full Brillouin zone for different chemical potentials $E_f = 1.33, 1.43, 1.52, 1.68, 2.1, 2.11, 2.13, 2.15$ eV respectively.

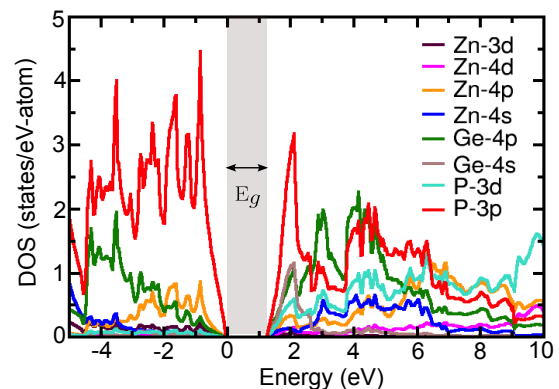


FIG. 4. Orbital projected partial density of states for different atoms in ZnGeP₂.

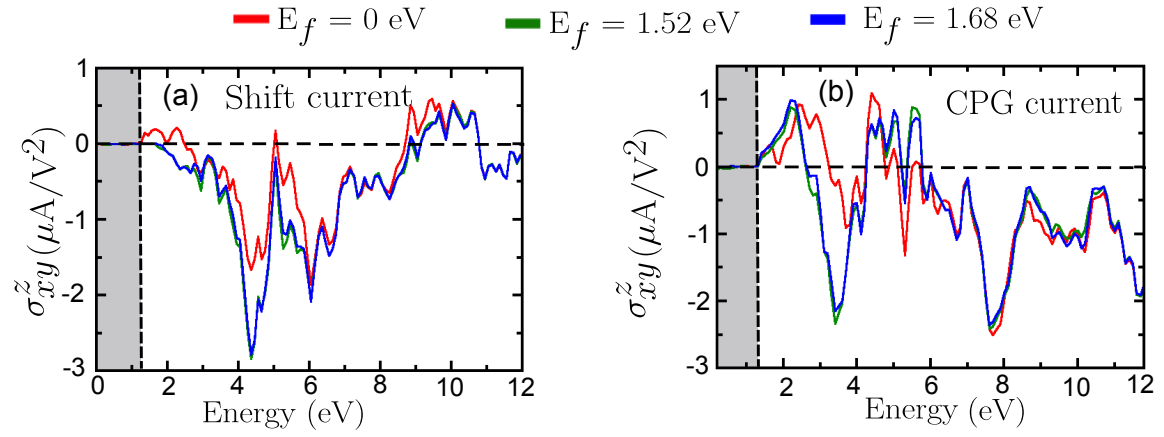


FIG. 5. σ_{xy}^z component of (a) shift current conductivities and (b) CPG current conductivities for different chemical potentials E_f .

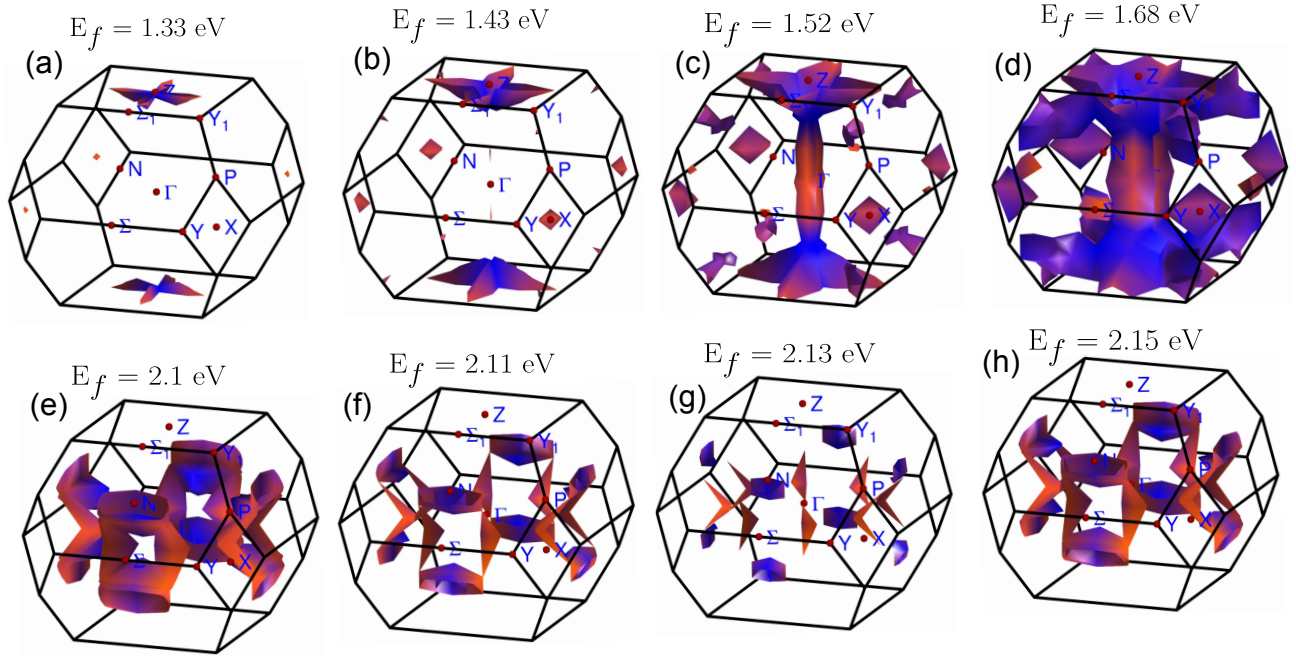


FIG. 6. (a)-(h) Calculated 3D Fermi surface for ZnGeP_2 in full Brillouin zone with different chemical potentials E_f .